MRS. RISTO OLAVI JUVONEN (Orcid ID : 0000-0001-9240-7673)

MR. ELMERI JOKINEN (Orcid ID : 0000-0003-2352-6550)

PROFESSOR OLLI PENTIKÄINEN (Orcid ID : 0000-0001-7188-4016)

Article type : Research Article

Corresponding author email id: risto.juvonen@uef.fi

Inhibition of human CYP1 enzymes by a classical inhibitor α-naphthoflavone and a novel inhibitor N-(3, 5- dichlorophenyl)cyclopropanecarboxamide - an in vitro and in silico study

The short running title: Inhibition of human CYP1 enzymes

Risto Olavi Juvonen[1], Elmeri Matias Jokinen[2], Adeel Javaid[1], Marko Lehtonen[1,3], Hannu Raunio[1], Olli Taneli Pentikäinen[2]

[1]School of Pharmacy, Faculty of Health Sciences, University of Eastern Finland, Kuopio, Finland

[2] Institute of Biomedicine, Faculty of Medicine, Integrative Physiology and Pharmacology, University of Turku, Kiinamyllynkatu 10, FI-20520 Turku, Finland

This article has been accepted for publication and undergone full peer review but has not been through the copyediting, typesetting, pagination and proofreading process, which may lead to differences between this version and the Version of Record. Please cite this article as doi: 10.1111/cbdd.13669

[3] LC-MS Metabolomics Center, Biocenter Kuopio, Kuopio, Finland

Acknowledgements

We thank Ms Hannele Jaatinen for excellent expertise in laboratory work. This work was supported by the Academy of Finland (grant no. 137589), the Finnish Cultural Foundation, Varsinais-Suomi Regional fund (E.M.J: 85182232) and by the Sigrid Juselius Foundation (grant no. 4704583). Finnish IT Centre for Science (CSC) is acknowledged for generous computational grant (O.T.P.: jyy2516 and jyy2585).

Data Availability Statement

The data that support the findings of this study are available on request from the corresponding author. The absence data could be found in supplementary information.

Abstract

Enzymes in the cytochrome P450 family 1 (CYP1) catalyze metabolic activation of procarcinogens and deactivation of certain anticancer drugs. Inhibition of these enzymes is a potential approach for cancer chemoprevention and treatment of CYP1-mediated drug resistance. We characterized inhibition of human CYP1A1, CYP1A2 and CYP1B1 enzymes by the novel inhibitor N-(3,5-dichlorophenyl) cyclopropanecarboxamide (DCPCC) and α-naphthoflavone (ANF). Depending on substrate, IC_{50} values of DCPCC for CYP1A1 or CYP1B1 were 10–95 times higher than for CYP1A2. IC_{50} of DCPCC for CYP1A2 was 100-fold lower than for enzymes in CYP2 and CYP3 families. DCPCC IC_{50} values were 10–680 times higher than the ones of ANF. DCPCC was a mixed type inhibitor of CYP1A2. ANF was a competitive tight-binding inhibitor of CYP1A1, CYP1A2 and CYP1B1. CYP1A1 oxidized DCPCC more rapidly than CYP1A2 or CYP1B1 to the same metabolite. Molecular dynamics simulations and binding free energy calculations explained the differences of binding of DCPCC and ANF to the active sites of all three CYP1 enzymes. We conclude that DCPCC is a more selective inhibitor for CYP1A2 than ANF. DCPCC is a candidate structure to modulate CYP1A2 mediated metabolism of procarcinogens and anticancer drugs.

Keywords: human, CYP, inhibition, α-naphthoflavone, N-(3,5-dichlorophenyl) cyclopropanecarboxamide, mechanism

Introduction

Compounds that are foreign to the body (xenobiotics) are transformed in oxidizing, reducing, hydrolyzing and conjugation reactions to water-soluble metabolites, which are excreted to urine or bile (Gonzalez, Coughtrie & Tukey, 2018). In xenobiotic metabolism, the cytochrome P450 (CYP) enzymes are particularly important, because they are abundant in the human liver and transform a more diverse array of xenobiotics than any other group of metabolic enzymes (Nebert & Russell, 2002; Testa, Pedretti, & Vistoli, 2012).

Human CYP1 family consists of CYP1A1, CYP1A2 and CYP1B1 enzymes, which differ in substrate and inhibitor selectivity. CYP1A2 is an abundant enzyme in the liver, while CYP1A1 and CYP1B1 are expressed preferentially in extrahepatic tissues. The amino acid sequence identity between CYP1A1 and CYP1A2 is 80%. Although the identity between CYP1As and CYP1B1 is relatively low (< 40%), there is a substantial substrate overlap. All three CYP1 family enzymes possess relatively small binding cavities, to which planar substrates such as melatonin, polycyclic aromatic hydrocarbons and xanthines fit well (Dutkiewicz & Mikstacka, 2018; Raunio, Kuusisto, Juvonen, & Pentikainen, 2015; Sridhar, Goyal, Liu, & Foroozesh, 2017; Zhou, Wang, Yang, & Liu, 2010).

A recent survey by Rendic and Guengerich (Rendic & Guengerich, 2015) showed that CYP1A2 participates in the metabolism of 10% of all chemicals (drugs, endogenous compounds, and general chemicals), whereas CYP1A1 and CYP1B1 are involved in the metabolism of 7% and 3% of all chemicals, respectively. These three CYP1 enzymes play a dominant role either in the metabolic activation or inactivation of numerous chemical carcinogens, such as aryl hydrocarbons and aromatic amines (Lewis & Ito, 2010; Pelkonen et al., 2008; Rendic & Guengerich, 2012).

Furafylline and α-naphthoflavone (ANF) are classical CYP1A2 inhibitors. Furafylline inhibits the enzyme in both competitive and mechanism-based manner. Based on indirect assays, furafylline does not inhibit other major human liver CYP forms. However, there is no data about inhibition of extrahepatic CYP1A1 and CYP1B1 by furafylline. ANF is a potent inhibitor of CYP1A2, but it also inhibits potently both CYP1A1 and CYP1B1 (Khojasteh, Prabhu, Kenny, Halladay, & Lu, 2011). Some clinically used drugs such as fluvoxamine are potent, but non-selective CYP1A2 inhibitors (Zhou et al., 2010). Thus, there is a need for a chemical inhibitor having selectivity within the CYP1 family enzymes. Numerous studies have been directed at finding potent and selective inhibitors of CYP1 family enzymes. The evaluated scaffolds include flavonoids, trans-stilbenes, coumarins, terpenoids, alkaloids, quinones, isothiocyanates and synthetic aromatics (Cui & Li, 2014; Foroozesh, Sridhar, Goyal, & Liu, 2019). Typically, these studies have included 2

out of 3 CYP1 family members, and effects of the candidate inhibitors on other human CYP forms have not been assessed.

Compared with CYP1A1 and CYP1B1, CYP1A2 is highly active in the bioactivation of carcinogenic heterocyclic and aromatic amines, such as 4-aminobiphenyl, 2-acetylaminofluorene and 2-amino-3-methyl-imidazo[4,5-f]quinoline. In addition, metabolism of anticancer agents by CYP1 enzymes is considered one of the reasons for anticancer drug resistance. CYP1A2 is involved in metabolism of e.g. erlotinib, etoposide and dacarbazine (Cui & Li, 2014; Nebert & Dalton, 2006). Discovery of a potent and selective inhibitor of CYP1A2 would serve two purposes: 1) Such an inhibitor could be used in in vitro assays with human liver microsomes to evaluate the contribution of CYP1A2 to metabolism of drug candidates in early nonclinical development (Fowler et al., 2017; Korhonen et al., 2005; Pelkonen et al., 2008). 2) The inhibitor could be used as a chemopreventive agent to suppress formation of reactive intermediates from procarcinogenic compounds, and treatment of CYP1A2-mediated drug resistance (Cui & Li, 2014; Go, Hwang, & Choi, 2015; Swanson et al., 2010). In addition, inhibitors are important tools to study catalytic properties of CYP enzymes to produce structure-activity relationship information for molecular modelling.

We discovered recently a novel potent inhibitor of CYP1A2, N-(3,5-dichlorophenyl)cyclopropane carboxamine (DCPCC). DCPCC is selective for CYP1A2 as it does not inhibit CYP2A6 or CYP2B6, two other enzymes with spatially restricted binding cavities (Raunio, Juvonen, Poso, Lahtela-Kakkonen, & Rahnasto-Rilla, 2016). The main aim of the present study was to characterize in detail the CYP1A1, CYP1A2 and CYP1B1 inhibition properties of DCPCC and compare them with those of ANF, a classical inhibitor of CYP1 enzymes (Figure 1A). DCPCC was also tested directly for its inhibition potency towards all major human xenobiotic-metabolizing enzymes. We used the profluorescent 7-ethoxyresorufin and novel coumarin derivatives as model substrates (Figure 1B) (Juvonen, Ahinko, Huuskonen, Raunio, & Pentikäinen, 2018). In silico modelling approaches were used to characterize the binding modes of DCPCC and ANF at the active sites of CYP1A1, CYP1A2 and CYP1B1.

Materials and methods

Chemicals. DCPCC was from Maybridge Thermo Fisher. Formic acid (99 %) and $MgCl_2$ were from Honeywell Riedel-de Haen (Bucharest, Romania). Acetonitrile (Ultra gradient HPLC grade), methanol (HPLC gradient grade) and glycine were from Fisher J.T. Baker (Waltham, Massachusetts). Ethanol (≥ 99.5%, Etax Aa) was from Altia (Helsinki, Finland). Water was deionized by MilliQ gradient A10. All chemicals were of the highest purity available from their commercial suppliers. ANF, 7-ethoxyresorufin,

resorufin, Tris-HCl, $MnCl_2$, $MgCl_2$, isocitric acid and isocitric acid dehydrogenase were purchased from Sigma-Aldrich (Steinheim, Germany), KCl from J.T. Baker, NADPH and NADP+ from Roche Diagnostics (Mannheim, Germany). 200 mL NADPH regenerating system contained 178.5 mg $NADP^+$ (nicotinamide adenine dinucleotide phosphate), 645 mg isocitric acid, 340 mg KCl, 240 mg $MgCl_2$, 0.32 mg $MnCl_2$ and 15 U isocitric acid dehydrogenase.

Coumarin derivatives: Synthesis and experimental data for compounds **1**-**6** (3-(4-trifluoromethylphenyl)-6-methoxycoumarin (**1**), 3-(4-ftrifluoromethoxyphenyl)-7-methoxycoumarin (**2**), 3-(3-hydroxyphenyl)-6-hydroxycoumarin (**3)**, 3-(3-methoxyphenyl)-7-methoxycoumarin (**4)**, 3-(3-methoxyphenyl)-6-methoxycoumarin (**5)**, 3-(3-benzyloxyphenyl)-7-methoxycoumarin (**6**) (Figure 1B) have been published earlier (Juvonen, Ahinko, Huuskonen, Raunio, & Pentikainen, 2019; Niinivehmas et al., 2018; Rauhamäki et al., 2018).

Biological material. Baculovirus-insect cell-expressed human CYP1A1, CYP1A2, CYP1B1, CYP2A6, CYP2B6, CYP2C8, CYP2C9, CYP2C19, CYP2D6, CYP2E1, CYP3A4, CYP3A5 and CYP3A7 were purchased from BD Biosciences Discovery Labware (Woburn, MA, USA) and used according to the manufacturer's instructions.

Oxidation assays. The kinetic assays were carried out in 100 µL volume containing 100 mM Tris-HCl buffer pH 7.4, 0–40 µM coumarin derivative or 0–10 µM 7-ethoxyresorufin, 1–25 nM recombinant CYP or 0–0.1 g/L microsomal protein and 20 % NADPH regenerating system (Figure 1). Incubations took place at 37°C in 96-multiwell plates; the fluorescence was measured with a Victor2 plate reader (PerkinElmer Life Sciences, Turku, Finland). The detailed conditions are described in the Figures and Tables. The reaction was started by adding NADPH and fluorescence was measured at 2-min intervals for 40 min using excitation 405 nm and emission 460 nm for oxidation of coumarin derivatives and excitation 570 nm and emission 615 nm for 7-ethoxyresorufin or 7-pentoxyresorufin O-dealkylations. Incubations without substrate, enzyme or NADPH were used as blank reactions. Resorufin was used as a standard and 7-hydroxycoumarin as the surrogate standards to calculate the amount of product formed. The linear phase of the reactions was used for calculations.

Inhibition. When the oxidation of coumarin derivatives was inhibited by 3.2 nM – 20 µM ANF or 20 nM – 20 µM DCPCC, the same incubation conditions and measurement setup as described above was used. One µL ANF or DCPCC was added from 100% dimethyl sulfoxide stock solution. Non-inhibited sample contained 1% dimethyl sulfoxide, and negative control did not contain microsomes.

Oxidation of DCPCC. 10 µM DCPCC was incubated in 100 µL 100 mM Tris-HCl pH 7.4 containing 10 nM CYP1A1, 2 nM CYP1A2 or 10 nM CYP1B1 and 20 % NADPH regenerating system at 37°C. 300 µL acetonitrile was applied at different time-points within 0–60 min to stop the reaction. The mixture was centrifuged for 5 min at 10 000 x g, the supernatant was transferred to an Eppendorf tube and stored at –80°C for the analysis by Orbitrap ultra-high performance liquid chromatography-mass spectrometry (UHPLC-MS).

Analysis by Orbitrap UHPLC-MS. Targeted metabolite profiling analysis was carried out at the LC-MS metabolomics center (Biocenter Kuopio, University of Eastern Finland). The analysis was carried out with the Vanquich Flex UHPLC system (Thermo Scientific, Bremen, Germany) coupled online to high-resolution mass spectrometer (Q Exactive Focus, Thermo Scientific, Bremen, Germany). Samples were analyzed using a reversed-phase chromatographic technique. The sample solution (2 µl) was injected onto a column (Zorbax Eclipse XDBC18, 2.1 × 100 mm, 1.8 µm, Agilent Technologies, Palo Alto, CA, USA) that was kept at 40°C. Mobile phases, delivered at 400 µL/min, consisted of water (eluent A) and methanol (eluent B), both containing 0.1 % (v/v) of formic acid. The following gradient profile was used: 0–10 min: 2 to 100% B, 10–14.50 min: 100% B, 14.50–14.51 min: 100 to 2% B; 14.51–20 min: 2% B. The sample tray was at 10°C during these analyses.

Mass spectrometer was equipped with heated electrospray ionization, and the positive ionization mode was used to acquire the data. The following ionization source settings were utilized; spray voltage (3.5 kV), sheath gas (40), auxiliary gas (10), and sweep gas (2) (flow rates as arbitrary units for ion source). The capillary temperature and the probe heater temperature were both set to 300°C. The S-lens RF level was set to 50 V. A full scan range from 120 to 1100 (m/z) was used with the resolution of 70 000 (m/Δm, full width at half maximum at 200 u). Automatic injection time was used, and Automated Gain Control (AGC) was targeted at 1 000 000 ions. The detector was calibrated before the sample sequence and subsequently operated at high mass accuracy (<2 ppm).

TraceFinder 4.1 software (Thermo Scientific, Bremen, Germany) was used for data processing and visualization. The identification of DCPCC and its oxidation metabolites were based on the accurate mass and isotope information. In addition, DCPCC was identified with an authentic standard compound by comparison of retention times present in the standard and samples.

Modelling of CYP1 enzymes and docking of inhibitors. Crystal structures of CYP1A1, CYP1A2 and CYP1B1 in complex with ANF were obtained from Protein Data Bank (Berman et al., 2000) (1A1: 4I8V (Walsh, Szklarz, & Scott, 2013); 1A2: 2HI4 (Sansen et al., 2007); 1B1: 3PM0 (A. Wang, Savas, Stout, & Johnson,

2011). A-chains of the CYP1 structures were aligned using VERTAA in BODIL molecular modelling environment (Lehtonen et al., 2004), and these structures were used in molecular docking. Prior to docking, hydrogens were added to the protein structures with REDUCE (Word, Lovell, Richardson, & Richardson, 1999). DCPCC and ANF were drawn with MAESTRO (v. 11.5.011, Release 2018-1, Schrödinger, LLC, New York, USA). LIGPREP module of MAESTRO was used to prepare the compounds with the following settings: OPLS3 force field (Harder et al., 2016); protonation at pH 7.4 and molecule ionization using EPIK (Shelley et al., 2007); generation of a maximum number of 32 tautomers and stereoisomers per inhibitor. LIGPREP generated a single structure for both compounds. Docking was performed with the PLANTS software (Korb, Stützle, & Exner, 2009). ANF bound in each CYP1 crystal structure was used to obtain coordinates of the center of the binding cavity. Binding site radius was set to 10 Å. Ten best-scored docking poses were acquired from each CYP1's docking with cluster rmsd 2.5 Å, totaling 30 docking poses per inhibitor.

Molecular dynamics simulations. All docking complexes of DCPCC or ANF with each CYP1 form were used as starting structures for molecular dynamics (MD) simulations. Partial charges for the ligands were derived using GAUSSIAN 16 (RevB.01, Gaussian, Inc., Wallingford, CT, 2016). Geometry optimization with polarizable continuum solvent model and calculations of the electrostatic potential were conducted at the HF/6-31G* level. The atom-centered point charges were calculated from the electrostatic potentials using the RESP method (Bayly, Cieplak, Cornell, & Kollman, 1993).

The AMBER18 package (University of California, San Francisco, Case et al., 2018) was used to set up the simulation system: generation of ff14SB force field (Maier et al., 2015) parameters for protein; combining protein and inhibitor parameterizations; solvation of the protein-ligand complex with a cubic box of TIP3P water molecules (Jorgensen, Chandrasekhar, Madura, Impey, & Klein, 1983) extending 15 Å away from the protein atoms in all dimensions. The system was neutralized by adding Cl^- counter ions. Penta-coordinate ferric high-spin parameters (Shahrokh, Orendt, Yost, & Cheatham, 2012) and the general AMBER force field (J. Wang, Wolf, Caldwell, Kollman, & Case, 2004), both provided in AMBER18, were used for the heme group and the proximal cysteine ligand in each CYP1 structure.

MD simulations were performed with NAMD 2.12 (Phillips et al., 2005). First, a four-step energy minimization was performed using the conjugate gradient method: 1. 5000 steps with all atoms except hydrogens restrained (restraining force 1 kcal/mol); 2. 5000 steps with all atoms except hydrogens and solvent molecules restrained; 3. 10 000 steps with only protein backbone atoms restrained; 4. 5000 steps with no restraints. Next, the systems were heated to 300 K while keeping protein backbone atoms restrained (4 kcal/mol). 2 ns of MD with protein backbone atoms restrained was run. The restraining force

was gradually decreased every 500 ps, starting with 4 kcal/mol. Finally, a 10 ns production simulation was performed with 2 fs time step, without restraints, in the NPT ensemble (1 atm). All simulations were performed with the periodic boundary conditions, using 12 Å cutoff for nonbonded interactions and particle mesh Ewald summation (Darden, York, & Pedersen, 1993; Essmann et al., 1995) for long-range electrostatic interactions.

Molecular mechanics/Generalized Born surface area calculations. MM/GBSA analyses were performed with MMPBSA.py (Miller et al., 2012) distributed within AMBER18. CPPTRAJ (Roe & Cheatham, 2013) was used in trajectory processing before the MM/GBSA calculations. The Generalized Born calculations were based on the igb5 model (Onufriev, Bashford, & Case, 2004). The general scheme for estimating binding free energies of protein-ligand complexes with MM/GBSA is the following: $DG_{bind} = G_{comp} – G_{prot} – G_{lig}$, where DG_{bind} is the binding free energy, and G_{comp}, G_{prot} and G_{lig} are the free energies of the complex, protein and ligand, respectively. Estimation of the energies was performed according to the equation: $DE_{MM} + DG_{GB} + DG_{nonpolar} – TDS$, where DE_{MM} is the gas-phase interaction energy between the CYP1 and the inhibitor, including both electrostatic and van der Waals energies; DG_{GB} and $DG_{nonpolar}$ represent the polar and nonpolar components of the desolvation free energy; TDS is the change of conformational entropy which was not considered here because of its high computational cost. DG_{bind} was calculated for every simulation snapshot and averaged to obtain DG_{total}. DG_{total} of different ligand binding modes can be used as an estimation of the relative binding affinity to identify the most probable binding modes (Ahinko, Niinivehmas, Jokinen, & Pentikäinen, 2019; Hou, Wang, Li, & Wang, 2011).

Figure preparation. Figures 7-9 were prepared using BODIL molecular modelling environment (Lehtonen et al., 2004) and MOLSCRIPT (Kraulis, 1991) with RASTER3D (Merritt & Murphy, 1994).

Results

Inhibition of CYP enzymes by DCPCC and ANF

Our earlier study indicated that DCPCC inhibits potently CYP1A2, but not CYP2A6 or CYP2B6 (Raunio et al., 2016). The present study first evaluated the inhibition of 9 other human CYP enzymes by DCPCC (Table 1). DCPCC inhibited CYP1A2 by 50 % at 100 nM level, whereas more than 10 µM concentration was needed to inhibit CYPs 2A6, 2B6, 2C8, 2C9, 2C19, 2D6, 2E1, 3A4 or 3A5.

Next, inhibition characteristics of CYP1A1, CYP1A2 and CYP1B1 by DCPCC and ANF were assessed in more detail using oxidation of 7-ethoxyresorufin and the coumarin derivative **5** as probe reactions (Figure 2 and Table 2). The IC_{50} values of DCPCC for CYP1A1, CYP1B1 and CYP1A2 were 10–680 times higher than those

of ANF. Based on IC_{50} ratios DCPCC was 58-fold and 21-fold more potent in inhibiting CYP1A2 than CYP1A1 and CYP1B1, respectively, with **5** as substrate. In contrast, ANF was the most potent against CYP1B1 and only little more potent against CYP1A2 than CYP1A1 (Table 2). These data indicated that ANF was a more potent inhibitor than DCPCC against CYP1 enzymes, but DCPCC showed inhibition selectivity for CYP1A2. ANF was the most potent inhibitor for CYP1B1 but was not selective.

The effects of preincubation of DCPCC and ANF with CYP1A2 enzyme and NADPH on inhibition were evaluated. Firstly, both ANF and DCPCC were incubated with CYP1A2 in the presence of NADPH and then added the probe substrate 7-ethoxyresorufin. Preincubation increased the IC_{50} of both DCPCC (0.15 → 0.8 μM) and ANF (5 → 50 nM) compared to the values obtained without preincubation (Figure 3). This demonstrated that neither DCPCC nor ANF are mechanism-based inhibitors of CYP1A2. The increase of IC_{50} value may due to oxidation of these inhibitors to inactive metabolites during the preincubation.

The IC_{50} of ANF and DCPCC for 7-ethoxyresorufin O-deethylation was determined at different concentrations of CYP1A1, CYP1A2 or CYP1B1 or human liver microsomal protein (Figure 4). The IC_{50} of ANF increased linearly when the concentration of CYP1 enzymes or liver microsomal protein increased. CYP1A2 concentration did not affect similarly the IC_{50} of DCPCC. In contrast, IC_{50} decreased at higher CYP1A2 or microsomal protein concentrations (Figure 4) and IC_{50} of DCPCC against CYP1A1 and CYP1B1 is at micromolar level, demonstrating that ANF is a tight-binding inhibitor of CYP1A1, CYP1A2 and CYP1B1, while DCPCC is not.

To reveal the inhibition mechanism, inhibition of CYP1A1, CYP1A2 and CYP1B1 catalyzed reactions by ANF and DCPCC were assessed at different concentrations of 7-ethoxyresorufin or six coumarin derivatives (Table 3 and Supplement Figure 1). The apparent Michaelis-Menten parameters of both V_{max}/K_m and $1/V_{max}$ were linearly dependent on the concentration of DCPCC, indicating that DCPCC is a mixed-type inhibitor of CYP1A2. In the six probe reactions, competitive inhibition constant values were lower than the uncompetitive inhibition ones. The ratio of K_{iu}/K_{ic} varied from 1.1 to 23. DCPCC was a competitive inhibitor of CYP1A2 oxidation of compound **6**, as the apparent V_{max}/K_m was linearly dependent on the concentration of DCPCC, and $1/V_{max}$ was not dependent on DCPCC concentration.

ANF appeared to be a competitive inhibitor for all CYP1 catalyzed 7-ethoxyresorufin O-deethylation reactions, as the IC_{50} value increased linearly when substrate concentration was increased (Figure 5). K_{ic} value of ANF was lowest for CYP1A1 catalyzed reaction, being 80 times higher for CYP1B1, and 180 times higher for CYP1A2 catalyzed reaction (Table 4).

Oxidative metabolism of DCPCC by human CYP1 enzymes

We also evaluated the oxidation of DCPCC by recombinant human CYP1 enzymes. DCPCC was incubated at CYP oxidation conditions for 60 min at 37°C and then analyzed by Orbitrap HPLC-MS. Only 1 oxidized metabolite of m/z 243.9933–243.9940 (expected m/z 243.9938, m/z of DCPCC + O) was observed. Its peak area was increased time-dependently. CYP1A1 produced 10 times more of this metabolite than CYP1A2 or CYP1B1 (Figure 6).

Docking/modelling of ANF and DCPCC in the active sites of CYP1 enzymes

Molecular docking, MD simulations and subsequent MM/GBSA binding free energy calculations were used to identify the most probable DCPCC binding mode in the active site of each of the CYP1 forms. The focus here was especially on providing mechanical background for the experimental IC_{50} and rate of metabolism results. The same protocol was performed with ANF, and the results were compared to the existing crystal structure and site of metabolism data of ANF-CYP1 complexes.

Binding of DCPCC

MM/GBSA calculations predicted that DCPCC binds to the active site of CYP1A2 more potently than to CYP1A1 or CYP1B1. The predicted DG_{total} values for the lowest energy systems were -35.5 kcal/mol for 1A1, -38.0 kcal/mol for 1A2 and -33.0 kcal/mol for 1B1. When this result is compared to experimental IC_{50} measurements, it can be seen that the prediction is consistent for CYP1A2, but the rank order is different between CYP1A1 and CYP1B1 (Table 2).

In the predicted binding modes of DCPCC with each CYP1 form, the compound was observed in an orientation where the cyclopropane ring was pointing towards the heme group (Figure 7). In the DCPCC-CYP1A1/1A2 complexes, DCPCC expressed such binding mode throughout the simulation. In the complex formed with CYP1B1, DCPCC was initially positioned far from the heme in a transverse orientation but adopted a pose described above during the simulation (Figure 7). Based on all 10 simulations per CYP1 form, starting poses with the cyclopropane closest to the heme were generally well retained and had the lowest DG_{total} values (Table S1; Figure S2; Figure S3; Figure S4). Poses with dichlorophenyl closest to the heme were predicted less probable due to generally higher DG_{total} values than the cyclopropane orientations. Distant and transverse starting poses moved closer to the heme and obtained either of the orientations mentioned above during the simulations (Table S1).

DCPCC-CYP1A1 and DCPCC-CYP1A2 complexes expressed highly similar interaction patterns in their low energy binding modes. In both complexes, DG_{bind} stabilized after the formation of a hydrogen bond between DCPCC's amide group and Ser122 in CYP1A1 and Thr124 in the corresponding position in CYP1A2

(Figure 7; Figure S2; Figure S3). The binding mode of DCPCC was further stabilized by π-stacking interactions between the dichlorophenyl and Phe123 or Phe224 in CYP1A1 and Phe125 or Phe226 in CYP1A2. Multiple hydrophobic interactions were observed between the cyclopropane and the residues around the heme group (1A1: Ile386, Leu496, Ala317, Thr321; 1A2: Thr124, Ile386, Thr321, Leu382, Ala317).

Despite having highly similar binding modes, slight, but crucial differences were observed between the DCPCC-CYP1A1/1A2 complexes in the positioning of the cyclopropane above the heme group. Methyl group of Thr124 in CYP1A2 was observed to force the side chain of Ile386 to a conformation where it occupied space over the heme group. Due to this, the cyclopropane was pushed towards the center of the heme group, covering more of the Fe atom than in the DCPCC-CYP1A1 complex (Figure 8). Secondly, the methyl group of Thr321 was orientated towards the cyclopropane in the DCPCC-CYP1A2 complex, forming a hydrophobic contact with the compound. In the DCPCC-CYP1A1 complex, the side chain of the corresponding threonine was orientated towards the heme group. Due to these differences, a small unoccupied area was present right next to the Fe atom and the cyclopropane (surrounded by the residues Ala317 and Thr321) in DCPCC-CYP1A1, but not in DCPCC-CYP1A2.

In the predicted binding mode of DCPCC in the active site of CYP1B1, DG_{bind} was seen to stabilize after a hydrogen bond formed between the amide group of DCPCC and Thr334 while the dichlorophenyl formed π-stacking interactions with Phe134 or Phe231 (Figure 7; Figure S4). Notably, the hydrogen bond formed to the opposite side of the active site than in the DCPCC-CYP1A1/1A2 complexes. In CYP1B1, Ala133 possesses the Ser122/Thr124 site, abolishing the possibility of DCPCC forming a hydrogen bond at this site. Due to this, the cyclopropane ring was shifted closer to Val395 and Thr334, leaving a small, unoccupied space above the heme Fe similarly as in the DCPCC-CYP1A1 complex. However, in the DCPCC-CYP1B1 complex, the cyclopropane was placed further away from the Fe atom than in DCPCC-CYP1A1. Average distance between DCPCC cyclopropane and heme Fe during the last 5 ns of the simulations was 4.8 Å for 1A1, 4.4 Å for 1A2 and 5.2 Å for 1B1 (Figure S5.

Binding of ANF

Based on the binding energy calculations, ANF was recognized as a more potent inhibitor of all CYP1 forms than DCPCC (the lowest ANF-CYP1 DG_{total} values: CYP1A1: -49.4; CYP1B1: -48.7; CYP1A2: -48.5 kcal/mol) (Table S2); Figure S6; Figure S7; Figure S8). Consistently with the experimental IC_{50} measurements, the small differences in the DG_{total} values showed ANF having no significant selectivity for any of the CYP1 forms.

As a bulkier molecule than DCPCC, ANF was not able to significantly change its initial orientation during any of the MD simulations. The predicted ANF binding pose in complex with CYP1A1 was highly similar to the ANF-CYP1A1 crystal structure (PDB: 4I8V; Figure 9). As in the crystal structure, the phenyl ring was orientated towards the heme group, while the benzo(h)chromen-4-one moiety formed π-stacking interactions with Phe224. A hydrogen bond was observed between Asn222 and the carbonyl oxygen of ANF.

For CYP1A2, the predicted binding mode differed clearly from the crystal structure pose (PDB: 2HI4; Figure 9). With CYP1A2, ANF adopted an orientation with the benzo(h)chromen-4-one orientated towards the heme group. A hydrogen bond formed between ANF's carbonyl oxygen and Thr498. The phenyl ring entered a region surrounded by Phe226, 260, and 256. Notably, the binding pose prediction most similar to the ANF-CYP1A2 crystal structure was ranked second by MM/GBSA, with only a 1.2 unit difference in DG_{total} (-47.3 kcal/mol). A water-mediated hydrogen bond was observed between Gly316 and the carbonyl oxygen of ANF in the 2nd-ranked complex. In addition, placement of the benzo(h)chromen-4-one system seemed more optimal for the π-stacking interactions, especially with Phe226, than in the best-ranked pose.

In the best-ranked ANF-CYP1B1 complex, ANF had a flipped orientation when compared to the crystal structure (PDB: 3PM0; Figure 9), expressing a binding mode similar to the ANF-CYP1A1/1A2 crystal structures. The carbonyl oxygen formed water-mediated hydrogen bonds with Asp333 and Lys512. The benzo(h)chromen-4-one moiety was well placed for forming π-stacking interactions with Phe231. The binding prediction with the best correspondence to the ANF-CYP1B1 crystal structure was ranked 6th by MM/GBSA with a clear difference in DG_{total} to the best-ranked pose (-42.5 kcal/mol for the 6th ranked complex).

Discussion

The inhibition characteristics of a novel CYP1A2 inhibitor DCPCC and the classical inhibitor ANF towards all 3 enzymes in the human CYP1 family were evaluated. ANF was a more potent inhibitor of CYP1A1, CYP1B1 and CYP1A2 than DCPCC, but did not exhibit selectivity for CYP1A2. DCPCC was selective for CYP1A2 with IC_{50} of 0.20–0.71 μM, and selectivity extended to all hepatic xenobiotic-metabolizing CYP enzymes. Neither inhibitor acted in a mechanism-based irreversible fashion. DCPCC was a mixed-type linear inhibitor of CYP1A2 inhibiting both by competitive and uncompetitive mechanisms. The competitive inhibition was dominant, as its inhibition constant was smaller than the uncompetitive one. As shown

previously for CYP1A2 (Cho et al., 2003), ANF was a tight-binding inhibitor of CYP1A1, CYP1A2 and CYP1B1.

Molecular modelling, docking and molecular dynamics data were consistent with the experimental results. The binding energy calculations recognized DCPCC as a more potent inhibitor of CYP1A2 than of CYP1A1 or CYP1B1, like the IC_{50} values of DCPCC against these CYPs. The inconsistent rank order of the binding energies of CYP1A1 and CYP1B1 could be affected by different rates of DCPCC metabolism by these two CYPs. DCPCC displayed both competitive and uncompetitive inhibitory activity towards CYP1A2. Uncompetitive inhibition mechanism may be caused by slow release of the formed oxidation product of DCPCC.

One oxidized metabolite was produced from DCPCC by all the human CYP1 enzymes, CYP1A1 being the most efficient catalyst. The cyclopropane ring was predicted to be the most probable DCPCC site of metabolism with all the CYP1 forms, since it was oriented toward to heme. Slight variation in positioning and distances of the cyclopropane above the heme group could explain differences between catalytic activities among the CYP1 forms. In DCPCC-CYP1A1, the hydroxyl group of Thr321 could stabilize the positioning of molecular oxygen on the observed unoccupied space to facilitate initiation of the reaction (Guengerich, 2007). Too close orientation around the heme group in DCPCC-CYP1A2 and the more distant positioning of the cyclopropane group in DCPCC-CYP1B1 could be non-optimal for the reaction rates.

In the predicted ANF-CYP1A2 complex, the benzo(h)chromen-4-one moiety was placed closest to the heme group. The benzo(h)chromen-4-one moiety has been reported as the primary site of slow CYP1-mediated metabolism of ANF, which indicates this as a possible binding orientation (Bauer et al., 1995). On the other hand, the ANF-CYP1A2 complex ranked 2nd by MM/GBSA was similar to the crystal structure pose and had only a small difference in the DG_{total} value. The best-ranked ANF-CYP1B1 complex displayed ANF binding mode highly similar to those seen in ANF-CYP1A1/1A2 crystal structures. Unmodeled electron density can be seen around ANF in the density difference map of CYP1B1 (PDB: 3PM0), which could suggest the presence of an alternative binding mode.

Of the classical inhibitors, furafylline inhibits CYP1A2 in both competitive and mechanism-based irreversible manner. As a competitive inhibitor, the K_i value of furafylline is 0.6–4.4 μM. Under pre-incubation conditions, the K_I value is 0.6–3.0 μM. Furafylline has selectivity against other human liver CYP forms, with IC_{50} values >100 μM when measured indirectly. However, there is no data about the inhibition of CYP1A1 and CYP1B1 by furafylline. ANF is a potent inhibitor of CYP1A2 with a K_i of 0.013 μM. However, ANF also inhibits potently both CYP1A1 and CYP1B1, with K_i of 0.01 μM and IC_{50} of 0.4–0.5 μM against

CYP1A1 and K_i of 0.0028 μM against CYP1B1. When measured indirectly, ANF has IC_{50} values >10 μM for all the other major human liver CYP forms (Khojasteh et al., 2011).

Liu and co-workers have published a series of studies describing coumarin or flavone derivatives with selectivity towards some of the 3 human CYP1 enzymes. 7-Ethynyl-3, 4, 8-trimethylcoumarin inhibited CYP1A1 and CYP1A2 without affecting CYP2A6 and CYP2B6 (Liu et al., 2012). A highly selective CYP1B1 inhibitor 5-hydroxy-4'-propargyloxyflavone was discovered. ANF-like and 5-hydroxyflavone derivatives preferentially inhibited CYP1A2, while β-naphthoflavone-like flavone derivatives showed selective inhibition of CYP1A1 (Liu et al., 2013). 7,8-furanoflavone time-dependently inhibited CYP1A2 with a K_i of 0.44 μM. With a 5-min preincubation, 0.01 μM 7,8-furanoflavone completely inactivates CYP1A2 but does not influence the activities of CYP1A1 and CYP1B1. 7,8-pyrano-4-trifluoromethylcoumarin was found to be a competitive inhibitor, showing high selectivity for the inhibition of CYP1A2 (K_i 0.39 μM) vs CYP1A1 and CYP1B1 (Liu et al., 2015). Inhibition of other human CYPs by these compounds was not evaluated. Recently novel ANF derivatives have been reported exhibiting potent and selective inhibition of CYP1B1 (Cui et al., 2015; Kubo, Yamamoto, & Itoh, 2019).

In conclusion, the CYP inhibition characteristics of DCPCC were evaluated in detail in vitro and in silico and compared with the classical inhibitor ANF. DCPCC was a mixed-type selective inhibitor of CYP1A2, and the selectivity also extended to all major human liver CYP forms. The binding mode predictions of DCPCC with CYP1A1, CYP1A2 and CYP1B1 provided highly detailed information about interactions at the enzyme active sites. These properties make DCPCC a good candidate for use as a CYP1A2 selective inhibitor when assessing in vitro the contribution of CYP1A2 in the metabolism of chemicals including drugs in human tissue samples. In addition, DCPCC could be used as a cancer chemopreventive agent and to suppress CYP1A2 mediated inactivation of specific drugs during cancer chemotherapy.

Conflict of interest: The authors confirm that this article content has no conflict of interest.

Figure legends

Figure 1. Structures of DCPCC and ANF (panel A) and the probe reactions (panel B). Non-fluorescent 7-ethoxyresorufin or coumarin derivative transforms via CYP-catalyzed oxidation to a fluorescent metabolite, which was measured in a 96 multiwell plate setup by fluorometer. Numbers assigned to the compounds: **1**, 3-(4-trifluoromethylphenyl)-6-methoxycoumarin; **2**, 3-(4-ftrifluoromethoxyphenyl)-7-methoxycoumarin; **3**, 3-(3-hydroxyphenyl)-6-hydroxycoumarin; **4**, 3-(3-methoxyphenyl)-7-methoxycoumarin; **5**, 3-(3-methoxyphenyl)-6-methoxycoumarin; **6**, 3-(3-benzyloxyphenyl)-7-methoxycoumarin.

Figure 2. Inhibition of oxidation of compound **5** and 7-ethoxyresorufin by DCPCC and ANF. Incubation mixture contained 10 µM **5** or 2.5 µM 7-ethoxyresorufin, 2.5 nM CYP1 enzymes, 20 % NADPH regenerating system, the indicated concentrations of DCPCC or ANF in 100 mM Tris-HCl pH 7.4. The 100% reaction samples contained solvent instead of the inhibitor, and blank samples did not contain any enzyme. Duplicate data points are relative to the activity without inhibitor.

Figure 3. Effect of preincubation of DCPCC (A) or ANF (B) on inhibition of CYP1A2 catalyzed 7-ethoxyresorufin O-deethylation. Different concentrations of DCPCC or ANF were incubated in the presence of 5 nM CYP1A2 and with (preincubation) or without (no preincubation) 20 % NADPH regenerating system in 100 mM Tris-HCl pH 7.4 at 37°C for 30 min, after which 2 µM 7-ethoxyresorufin was added and the incubation was continued for 40 min. Relative remaining activity (v_i/v_0, vi = rate in the presence of inhibitor, v_0 = rate without inhibitor (100%)) was calculated from the resorufin formation rate during the second incubation. The data was calculated from duplicate samples at every concentration.

Figure 4. Effect of amount of CYP1 enzymes on IC_{50} of ANF or DCPCC. Incubation mixture contained 2.5 µM ethoxyresorufin, the indicated concentration of enzymes or human microsomal protein, 20 % NADPH regenerating system, 0–0.1 µM ANF (A – D) or 0–1 µM DCPCC (E, F) in 100 mM Tris-HCl pH 7.4. The 100% reaction samples contained solvent instead of the inhibitor, and blank samples did not contain any enzyme.

Figure 5. Effect of 7-ethoxyresorufin concentration on ANF IC_{50} value. Incubation mixture contained the indicated concentrations of 7-ethoxyresorufin, 1 nM CYP1A1, 2.5 nM CYP1A2 or 2.5 nM CYP1B1, 20 % NADPH regenerating system, 0–1.2 µM ANF in 100 mM Tris-HCl pH 7.4. The 100% reaction contained solvent instead of the inhibitor and blank samples did not contain any enzyme.

Figure 6. Oxidation of DCPCC by CYP1 enzymes. 10 µM DCPCC was incubated in 100 µL 100 mM Tris-HCl pH 7.4 containing 10 nM CYP1A1 or 1B1 or 2 nM CYP1A2 enzyme and 20% NADPH regenerating system

for 60 min at 37°C and then analyzed by Orbitrap HPLC-MS. One metabolite was detected, whose normalized quantity is shown from duplicate samples.

Figure 7. Predicted binding modes of DCPCC with the CYP1 forms. On the top row, the initial molecular docking complexes of DCPCC with each CYP1 form can be seen. The predicted binding modes of DCPCC resulted via the binding energy calculations are at the bottom row. The atoms are colored as follows: C of DCPCC orange, C of heme group and surrounding residues cyan, O red, N blue, H white, Cl green, Fe yellow. Names and numbers of the surrounding residues are shown. The purple dashed lines indicate the hydrogen bonds formed between DCPCC and CYP1 residues.

Figure 8. Differences in the active site arrangements between the predicted DCPCC-CYP1A1 and DCPCC-CYP1A2 complexes. The binding mode of DCPCC with CYP1A1 and CYP1A2 is viewed from above the heme group. With CYP1A1, DCPCC can be seen to leave the Fe atom partially uncovered, whereas with CYP1A2 the cyclopropane group covers the Fe atom almost completely. The atoms are colored as follows: C of DCPCC orange, C of heme white, C of amino acids cyan, O red, N blue, chlorine green, Fe yellow.

Figure 9. Comparison of ANF's predicted and crystal structure binding modes. In each panel, the green ANF, heme group and residues are in conformations obtained from the MD simulations. The orange ANF represents the binding mode in the corresponding crystal structure (PDB-entries 4I8V, 2HI4 and 3PM0 for CYP1A1, 1A2 and 1B1, respectively). The purple dashed lines indicate the hydrogen bonds formed between ANF and CYP1 residues/water in the predicted binding modes. Heme group and residues are named and numbered and displayed as sticks with the following coloring: C cyan, O red, N blue, Fe yellow. In the rightmost panel, a water molecule is displayed as a red sphere (hydrogens not shown).

Table legends

Table 1. Selective inhibition of CYP1A2 by DCPCC among human hepatic CYP enzymes. Numbers in the Table indicate IC_{50} values of DCPCC. Incubation mixture contained 10 µM compounds **6, 4** or coumarin or 1 µM 7-pentoxyresorufin, 1 nM CYP enzymes, 0–20 µM DCPCC and 20 % NADPH regenerating system in 100 mM Tris-HCl pH 7.4.

Table 2. IC_{50} values of DCPCC and ANF for oxidation of compound **5** and 7-ethoxyresorufin. Incubation mixture contained 10 µM **5** or 2.5 µM 7-ethoxyresorufin, 2.5 nM CYP1 enzymes, different concentrations of DCPCC or ANF and 20 % NADPH regenerating system in 100 mM Tris-HCl pH 7.4. The 100 % reaction samples contained solvent instead of the inhibitor, and blank samples did not contain any enzyme. IC_{50}

values were calculated using the equation $v_i/v_0 = 1 / (1+I/IC_{50})$, in which v_i is rate at the concentration of inhibitor, v_0 is rate without inhibitor (100 % rate) and I is inhibitor concentration.

Table 3. Inhibition constants of DCPCC for CYP1A2 catalyzed reactions. Incubation mixture contained 0–40 µM of the indicated substrate, 2.5 nM CYP1A2 enzyme, 20% NADPH regenerating system and 0–1 µM DCPCC in 100 mM Tris-HCl pH 7.4. 100% reaction did not contain inhibitor, and blank samples did not contain CYP1. Secondary plots of the apparent Michaelis-Menten parameters V_{max}/K_m and $1/V_{max}$ of the reactions against DCPCC concentration are shown in supplement material (Figure 1_supplement).

Table 4. Competitive inhibition constants of ANF for CYP1 catalyzed 7-ethoxyresorufin O-deethylation. K_{ic} values were calculated from y-intercept (S = 0) of the linear regression lines of Figure 5, as competitive inhibitors obey the equation $IC_{50} = K_{ic} (1 + S/K_m) + E/2$. Concentration of CYP1A1 at the incubation was 1 nM, of CYP1A2 2.5 nM and of CYP1B1 2.5 nM.

References

Ahinko, M., Niinivehmas, S., Jokinen, E., & Pentikäinen, O. T. (2019). Suitability of MMGBSA for the selection of correct ligand binding modes from docking results. *Chemical Biology & Drug Design*, *93*, 522–538. https://doi.org/10.1111/cbdd.13446

Bauer, E., Guo, Z., Ueng, Y. F., Bell, L. C., Zeldin, D., & Guengerich, F. P. (1995). Oxidation of benzo[a]pyrene by recombinant human cytochrome P450 enzymes. *Chemical Research in Toxicology*, *8*, 136–142. https://doi.org/10.1021/tx00043a018

Bayly, C. I., Cieplak, P., Cornell, W., & Kollman, P. A. (1993). A well-behaved electrostatic potential based method using charge restraints for deriving atomic charges: the RESP model. *The Journal of Physical Chemistry*, *97*, 10269–10280. https://doi.org/10.1021/j100142a004

Berman, H. M., Westbrook, J., Feng, Z., Gilliland, G., Bhat, T. N., Weissig, H., … Bourne, P. E. (2000, January). The Protein Data Bank. *Nucleic Acids Research*, Vol. 28, pp. 235–242. Oxford, UK.

Cho, U. S., Park, E. Y., Dong, M. S., Park, B. S., Kim, K., & Kim, K. H. (2003). Tight-binding inhibition by alpha-naphthoflavone of human cytochrome P450 1A2. *Biochimica et Biophysica Acta*, *1648*, 195–202. https://doi.org/10.1016/s1570-9639(03)00148-1

Cui, J., & Li, S. (2014). Inhibitors and prodrugs targeting CYP1: a novel approach in cancer prevention and therapy. *Current Medicinal Chemistry*, *21*, 519–552. https://doi.org/10.2174/09298673113206660277

Cui, J., Meng, Q., Zhang, X., Cui, Q., Zhou, W., & Li, S. (2015). Design and Synthesis of New alpha-Naphthoflavones as Cytochrome P450 (CYP) 1B1 Inhibitors To Overcome Docetaxel-Resistance Associated with CYP1B1 Overexpression. *Journal of Medicinal Chemistry*, *58*, 3534–3547. https://doi.org/10.1021/acs.jmedchem.5b00265

Darden, T., York, D., & Pedersen, L. (1993). Particle mesh Ewald: An N·log(N) method for Ewald sums in large systems. *The Journal of Chemical Physics*, *98*, 10089–10092. https://doi.org/10.1063/1.464397

Dutkiewicz, Z., & Mikstacka, R. (2018). Structure-Based Drug Design for Cytochrome P450 Family 1 Inhibitors. *Bioinorganic Chemistry and Applications*, *2018*, 3924608. https://doi.org/10.1155/2018/3924608

Essmann, U., Perera, L., Berkowitz, M. L., Darden, T., Lee, H., & Pedersen, L. G. (1995). A smooth particle

mesh Ewald method. *The Journal of Chemical Physics*, *103*, 8577–8593. https://doi.org/10.1063/1.470117

Foroozesh, M., Sridhar, J., Goyal, N., & Liu, J. (2019). Coumarins and P450s, Studies Reported to-Date. *Molecules (Basel, Switzerland)*, *24*. https://doi.org/10.3390/molecules24081620

Fowler, S., Morcos, P. N., Cleary, Y., Martin-Facklam, M., Parrott, N., Gertz, M., & Yu, L. (2017). Progress in Prediction and Interpretation of Clinically Relevant Metabolic Drug-Drug Interactions: a Minireview Illustrating Recent Developments and Current Opportunities. *Current Pharmacology Reports*, *3*, 36–49. https://doi.org/10.1007/s40495-017-0082-5

Go, R.-E., Hwang, K.-A., & Choi, K.-C. (2015). Cytochrome P450 1 family and cancers. *The Journal of Steroid Biochemistry and Molecular Biology*, *147*, 24–30. https://doi.org/10.1016/j.jsbmb.2014.11.003

Guengerich, F. P. (2007). Mechanisms of cytochrome P450 substrate oxidation: MiniReview. *Journal of Biochemical and Molecular Toxicology*, *21*, 163–168.

Harder, E., Damm, W., Maple, J., Wu, C., Reboul, M., Xiang, J. Y., … Friesner, R. A. (2016). OPLS3: A Force Field Providing Broad Coverage of Drug-like Small Molecules and Proteins. *Journal of Chemical Theory and Computation*, *12*, 281–296. https://doi.org/10.1021/acs.jctc.5b00864

Hou, T., Wang, J., Li, Y., & Wang, W. (2011). Assessing the performance of the molecular mechanics/Poisson Boltzmann surface area and molecular mechanics/generalized Born surface area methods. II. The accuracy of ranking poses generated from docking. *Journal of Computational Chemistry*, *32*, 866–877. https://doi.org/10.1002/jcc.21666

Jorgensen, W. L., Chandrasekhar, J., Madura, J. D., Impey, R. W., & Klein, M. L. (1983). Comparison of simple potential functions for simulating liquid water. *The Journal of Chemical Physics*, *79*, 926–935. https://doi.org/10.1063/1.445869

Juvonen, R. O., Ahinko, M., Huuskonen, J., Raunio, H., & Pentikainen, O. T. (2019). Development of new Coumarin-based profluorescent substrates for human cytochrome P450 enzymes. *Xenobiotica; the Fate of Foreign Compounds in Biological Systems*, *49*, 1015–1024. https://doi.org/10.1080/00498254.2018.1530399

Juvonen, R. O., Ahinko, M., Huuskonen, J., Raunio, H., & Pentikäinen, O. T. (2018). Development of new Coumarin-based profluorescent substrates for human cytochrome P450 enzymes. *Xenobiotica; the Fate of Foreign Compounds in Biological Systems*, 1–10.

https://doi.org/10.1080/00498254.2018.1530399

Khojasteh, S. C., Prabhu, S., Kenny, J. R., Halladay, J. S., & Lu, A. Y. H. (2011). Chemical inhibitors of cytochrome P450 isoforms in human liver microsomes: a re-evaluation of P450 isoform selectivity. *European Journal of Drug Metabolism and Pharmacokinetics*, *36*, 1–16. https://doi.org/10.1007/s13318-011-0024-2

Korb, O., Stützle, T., & Exner, T. E. (2009). Empirical scoring functions for advanced protein-ligand docking with PLANTS. *Journal of Chemical Information and Modeling*, *49*, 84–96. https://doi.org/10.1021/ci800298z

Korhonen, L. E., Rahnasto, M., Mahonen, N. J., Wittekindt, C., Poso, A., Juvonen, R. O., & Raunio, H. (2005). Predictive three-dimensional quantitative structure-activity relationship of cytochrome P450 1A2 inhibitors. *Journal of Medicinal Chemistry*, *48*, 3808–3815. https://doi.org/10.1021/jm0489713

Kraulis, P. J. (1991). MOLSCRIPT: a program to produce both detailed and schematic plots of protein structures. *Journal of Applied Crystallography*, *24*, 946–950. https://doi.org/10.1107/S0021889891004399

Kubo, M., Yamamoto, K., & Itoh, T. (2019). Design and synthesis of selective CYP1B1 inhibitor via dearomatization of alpha-naphthoflavone. *Bioorganic & Medicinal Chemistry*, *27*, 285–304. https://doi.org/10.1016/j.bmc.2018.11.045

Lehtonen, J. V, Still, D.-J., Rantanen, V.-V., Ekholm, J., Björklund, D., Iftikhar, Z., … Johnson, M. S. (2004). BODIL: a molecular modeling environment for structure-function analysis and drug design. *Journal of Computer-Aided Molecular Design*, *18*, 401–419. Retrieved from http://www.ncbi.nlm.nih.gov/pubmed/15663001

Lewis, D. F. V, & Ito, Y. (2010). Human CYPs involved in drug metabolism: structures, substrates and binding affinities. *Expert Opinion on Drug Metabolism & Toxicology*, *6*, 661–674. https://doi.org/10.1517/17425251003674380

Liu, J., Nguyen, T. T., Dupart, P. S., Sridhar, J., Zhang, X., Zhu, N., … Foroozesh, M. (2012). 7-Ethynylcoumarins: selective inhibitors of human cytochrome P450s 1A1 and 1A2. *Chemical Research in Toxicology*, *25*, 1047–1057. https://doi.org/10.1021/tx300023p

Liu, J., Pham, P. T., Skripnikova, E. V, Zheng, S., Lovings, L. J., Wang, Y., … Foroozesh, M. (2015). A Ligand-Based Drug Design. Discovery of 4-Trifluoromethyl-7,8-pyranocoumarin as a Selective Inhibitor of

Human Cytochrome P450 1A2. *Journal of Medicinal Chemistry*, *58*, 6481–6493. https://doi.org/10.1021/acs.jmedchem.5b00494

Liu, J., Taylor, S. F., Dupart, P. S., Arnold, C. L., Sridhar, J., Jiang, Q., … Foroozesh, M. (2013). Pyranoflavones: a group of small-molecule probes for exploring the active site cavities of cytochrome P450 enzymes 1A1, 1A2, and 1B1. *Journal of Medicinal Chemistry*, *56*, 4082–4092. https://doi.org/10.1021/jm4003654

Maier, J. A., Martinez, C., Kasavajhala, K., Wickstrom, L., Hauser, K. E., & Simmerling, C. (2015). ff14SB: Improving the Accuracy of Protein Side Chain and Backbone Parameters from ff99SB. *Journal of Chemical Theory and Computation*, *11*, 3696–3713. https://doi.org/10.1021/acs.jctc.5b00255

Merritt, E. A., & Murphy, M. E. P. (1994). Raster3D Version 2.0. A program for photorealistic molecular graphics. *Acta Crystallographica Section D Biological Crystallography*, *50*, 869–873. https://doi.org/10.1107/S0907444994006396

Miller, B. R., McGee, T. D., Swails, J. M., Homeyer, N., Gohlke, H., & Roitberg, A. E. (2012). MMPBSA.py: An Efficient Program for End-State Free Energy Calculations. *Journal of Chemical Theory and Computation*, *8*, 3314–3321. https://doi.org/10.1021/ct300418h

Nebert, D. W., & Dalton, T. P. (2006). The role of cytochrome P450 enzymes in endogenous signalling pathways and environmental carcinogenesis. *Nature Reviews. Cancer*, *6*, 947–960. https://doi.org/10.1038/nrc2015

Nebert, D. W., & Russell, D. W. (2002). Clinical importance of the cytochromes P450. *Lancet (London, England)*, *360*, 1155–1162. https://doi.org/10.1016/S0140-6736(02)11203-7

Niinivehmas, S., Postila, P. A., Rauhamäki, S., Manivannan, E., Kortet, S., Ahinko, M., … Pentikäinen, O. T. (2018). Blocking oestradiol synthesis pathways with potent and selective coumarin derivatives. *Journal of Enzyme Inhibition and Medicinal Chemistry*, *33*, 743–754. https://doi.org/10.1080/14756366.2018.1452919

Onufriev, A., Bashford, D., & Case, D. A. (2004). Exploring protein native states and large-scale conformational changes with a modified generalized born model. *Proteins*, *55*, 383–394. https://doi.org/10.1002/prot.20033

Pelkonen, O., Turpeinen, M., Hakkola, J., Honkakoski, P., Hukkanen, J., & Raunio, H. (2008). Inhibition and induction of human cytochrome P450 enzymes: current status. *Archives of Toxicology*, *82*, 667–715.

https://doi.org/10.1007/s00204-008-0332-8

Phillips, J. C., Braun, R., Wang, W., Gumbart, J., Tajkhorshid, E., Villa, E., … Schulten, K. (2005). Scalable molecular dynamics with NAMD. *Journal of Computational Chemistry*, *26*, 1781–1802. https://doi.org/10.1002/jcc.20289

Rauhamäki, S., Postila, P. A., Niinivehmas, S., Kortet, S., Schildt, E., Pasanen, M., … Pentikäinen, O. T. (2018). Structure-Activity Relationship Analysis of 3-Phenylcoumarin-Based Monoamine Oxidase B Inhibitors. *Frontiers in Chemistry*, *6*, 1–18. https://doi.org/10.3389/fchem.2018.00041

Raunio, H., Juvonen, R. O., Poso, A., Lahtela-Kakkonen, M., & Rahnasto-Rilla, M. (2016). Common and Distinct Interactions of Chemical Inhibitors with Cytochrome P450 CYP1A2, CYP2A6 and CYP2B6 Enzymes. *Drug Metabolism Letters*, *10*, 56–64. https://doi.org/10.2174/1872312810666151204002456

Raunio, H., Kuusisto, M., Juvonen, R. O., & Pentikainen, O. T. (2015). Modeling of interactions between xenobiotics and cytochrome P450 (CYP) enzymes. *Frontiers in Pharmacology*, *6*, 123. https://doi.org/10.3389/fphar.2015.00123

Rendic, S., & Guengerich, F. P. (2012). Contributions of human enzymes in carcinogen metabolism. *Chemical Research in Toxicology*, *25*, 1316–1383. https://doi.org/10.1021/tx300132k

Rendic, S., & Guengerich, F. P. (2015). Survey of Human Oxidoreductases and Cytochrome P450 Enzymes Involved in the Metabolism of Xenobiotic and Natural Chemicals. *Chemical Research in Toxicology*, *28*, 38–42. https://doi.org/10.1021/tx500444e

Roe, D. R., & Cheatham, T. E. 3rd. (2013). PTRAJ and CPPTRAJ: Software for Processing and Analysis of Molecular Dynamics Trajectory Data. *Journal of Chemical Theory and Computation*, *9*, 3084–3095. https://doi.org/10.1021/ct400341p

Sansen, S., Yano, J. K., Reynald, R. L., Schoch, G. A., Griffin, K. J., Stout, C. D., & Johnson, E. F. (2007). Adaptations for the oxidation of polycyclic aromatic hydrocarbons exhibited by the structure of human P450 1A2. *The Journal of Biological Chemistry*, *282*, 14348–14355. https://doi.org/10.1074/jbc.M611692200

Shahrokh, K., Orendt, A., Yost, G. S., & Cheatham, T. E. 3rd. (2012). Quantum mechanically derived AMBER-compatible heme parameters for various states of the cytochrome P450 catalytic cycle. *Journal of Computational Chemistry*, *33*, 119–133. https://doi.org/10.1002/jcc.21922

Shelley, J. C., Cholleti, A., Frye, L. L., Greenwood, J. R., Timlin, M. R., & Uchimaya, M. (2007). Epik: a software program for pK(a) prediction and protonation state generation for drug-like molecules. *Journal of Computer-Aided Molecular Design*, *21*, 681–691. https://doi.org/10.1007/s10822-007-9133-z

Sridhar, J., Goyal, N., Liu, J., & Foroozesh, M. (2017). Review of Ligand Specificity Factors for CYP1A Subfamily Enzymes from Molecular Modeling Studies Reported to-Date. *Molecules (Basel, Switzerland)*, *22*. https://doi.org/10.3390/molecules22071143

Swanson, H. I., Njar, V. C. O., Yu, Z., Castro, D. J., Gonzalez, F. J., Williams, D. E., … Scott, E. E. (2010, April). Targeting drug-metabolizing enzymes for effective chemoprevention and chemotherapy. *Drug Metabolism and Disposition: The Biological Fate of Chemicals*, Vol. 38, pp. 539–544. https://doi.org/10.1124/dmd.109.031351

Testa, B., Pedretti, A., & Vistoli, G. (2012). Reactions and enzymes in the metabolism of drugs and other xenobiotics. *Drug Discovery Today*, *17*, 549–560. https://doi.org/10.1016/j.drudis.2012.01.017

Walsh, A. A., Szklarz, G. D., & Scott, E. E. (2013). Human cytochrome P450 1A1 structure and utility in understanding drug and xenobiotic metabolism. *The Journal of Biological Chemistry*, *288*, 12932–12943. https://doi.org/10.1074/jbc.M113.452953

Wang, A., Savas, U., Stout, C. D., & Johnson, E. F. (2011). Structural characterization of the complex between alpha-naphthoflavone and human cytochrome P450 1B1. *The Journal of Biological Chemistry*, *286*, 5736–5743. https://doi.org/10.1074/jbc.M110.204420

Wang, J., Wolf, R. M., Caldwell, J. W., Kollman, P. A., & Case, D. A. (2004). Development and testing of a general amber force field. *Journal of Computational Chemistry*, *25*, 1157–1174. https://doi.org/10.1002/jcc.20035

Word, J. M., Lovell, S. C., Richardson, J. S., & Richardson, D. C. (1999). Asparagine and Glutamine: Using Hydrogen Atom Contacts in the Choice of Side-chain Amide Orientation. *J . Mol . Biol*, *285*, 1735–1747. https://doi.org/10.1006/jmbi.1998.2401

Zhou, S.-F., Wang, B., Yang, L.-P., & Liu, J.-P. (2010). Structure, function, regulation and polymorphism and the clinical significance of human cytochrome P450 1A2. *Drug Metabolism Reviews*, *42*, 268–354. https://doi.org/10.3109/03602530903286476

Table 1. Selective inhibition of CYP1A2 by DCPCC among human hepatic CYP enzymes. Numbers in the Table indicate IC_{50} values of DCPCC. Incubation mixture contained 10 µM compounds **6, 4** or coumarin or 1 µM 7-pentoxyresorufin, 1 nM CYP enzymes, 0–20 µM DCPCC and 20 % NADPH regenerating system in 100 mM Tris-HCl pH 7.4.

CYP	**Substrate**			
	Compound 6	**Compound 4**	**Coumarin**	**7-pentoxy-resorufin**
1A2	130 nM	250 nM	-	-
2A6	-[a]	-	> 10 µM	-
2B6	-	-	-	> 10 µM
2C8	> 10 µM	-	-	-
2C9	> 10 µM	> 10 µM	-	-
C219	> 10 µM	-	-	-
2D6	> 10 µM	> 10 µM	-	-
2E1	> 10 µM	-	-	-
3A4	> 10 µM	-	-	-
3A5	> 10 µM	-	-	-

[a] CYP does not oxidize the substrate

Table 2. IC_{50} values of DCPCC and ANF for oxidation of compound **5** and 7-ethoxyresorufin. Incubation mixture contained 10 µM **5** or 2.5 µM 7-ethoxyresorufin, 2.5 nM CYP1 enzymes, different concentrations of DCPCC or ANF and 20 % NADPH regenerating system in 100 mM Tris-HCl pH 7.4. The 100 % reaction samples contained solvent instead of the inhibitor, and blank samples did not contain any enzyme. IC_{50} values were calculated using the equation $v_i/v_0 = 1 / (1+I/IC_{50})$, in which v_i is rate at the concentration of inhibitor, v_0 is rate without inhibitor (100 % rate) and I is inhibitor concentration.

Substrate	**CYP**	**DCPCC**	**ANF**	**IC_{50} ratio of DCPCC/ANF**	**IC_{50} ratio of CYP1/CYP1A2**	
		IC_{50} (95 % confidence limit) µM			*DCPCC*	*ANF*
Compound 5	CYP1A1	41 (3-78)	0.14 (0.12-0.15)	300	58	2
	CYP1A2	0.71 (0.52-0.89)	0.069 (0.053-0.085)	10	1	1
	CYP1B1	15 (9-20)	0.022 (0.02-0.025)	680	21	0.3
7-Ethoxy-resorufin	CYP1A1	19 (13-26	0.071 (0.062-0.079)	270	95	8
	CYP1A2	0.20 (0.16-0.25)	0.0088 (0.0063-0.011)	23	1	1

Table 3. Inhibition constants of DCPCC for CYP1A2 catalyzed reactions. Incubation mixture contained 0–40 µM of the indicated substrate, 2.5 nM CYP1A2 enzyme, 20% NADPH regenerating system and 0–1 µM DCPCC in 100 mM Tris-HCl pH 7.4. 100% reaction did not contain inhibitor, and blank samples did not contain CYP1. Secondary plots of the apparent Michaelis-Menten parameters V_{max}/K_m and $1/V_{max}$ of the reactions against DCPCC concentration are shown in supplement material (Figure 1_supplement).

Substrate	**K_{ic} (95 % confidence limit) nM**	**K_{iu} (95 % confidence limit) nM**	**Ratio of K_{iu}/K_{ic}**
Compound **3**	24 (0–93)	62 (12–140)	2.6
Compound **5**	39 (32–45)	880 (550–2200)	23
Compound **4**	290 (245–338)	1400 (1100–1700)	4.8
Compound **6**	680 (360–1400)	----	
Compound **1**	98 (43–190)	110 (93–120)	1.1
Compound **2**	32 (19–50)	52 (38–62)	1.6
7-Ethoxyresorufin	120 (74–180)	430 (310–640)	3.6

Table 4. Competitive inhibition constants of ANF for CYP1 catalyzed 7-ethoxyresorufin O-deethylation. K_{ic} values were calculated from y-intercept (S = 0) of the linear regression lines of Figure 5, as competitive inhibitors obey the equation $IC_{50} = K_{ic} (1 + S/K_m) + E/2$. Concentration of CYP1A1 at the incubation was 1 nM, of CYP1A2 2.5 nM and of CYP1B1 2.5 nM.

CYP1	**K_{ic} (95 % confidence limit) nM**
1A1	0.09 (0.021–0.16)
1A2	16 (14–19)
1B1	7.5 (6.9–8.1)

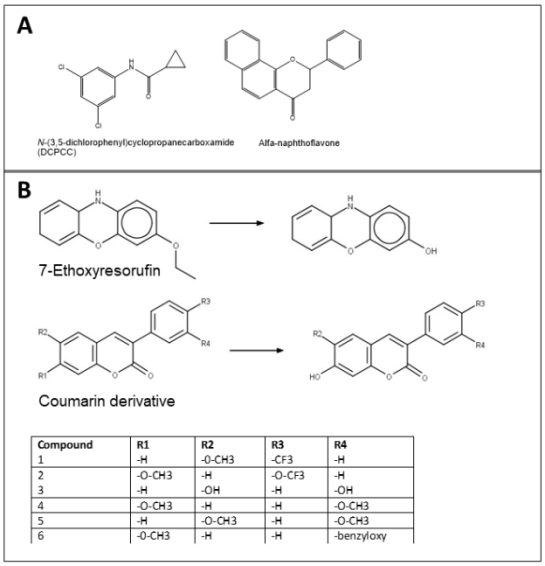

Compound	R1	R2	R3	R4
1	-H	-0-CH3	-CF3	-H
2	-O-CH3	-H	-O-CF3	-H
3	-H	-OH	-H	-OH
4	-O-CH3	-H	-H	-O-CH3
5	-H	-O-CH3	-H	-O-CH3
6	-0-CH3	-H	-H	-benzyloxy

Figure 1.

cbdd_13669_f1.tif

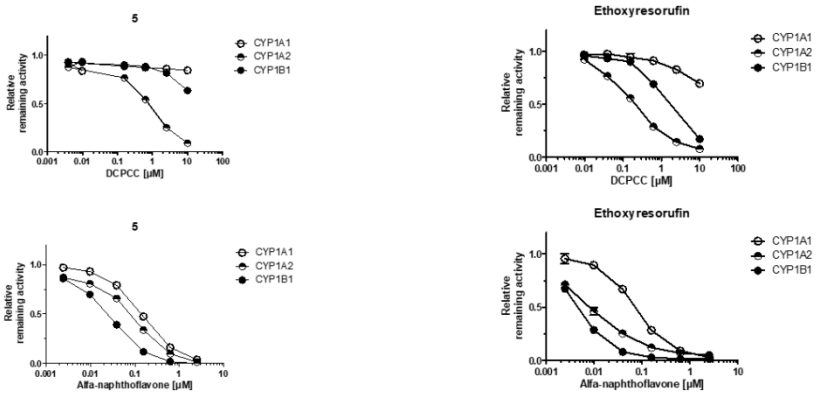

Figure 2.

cbdd_13669_f2.tif

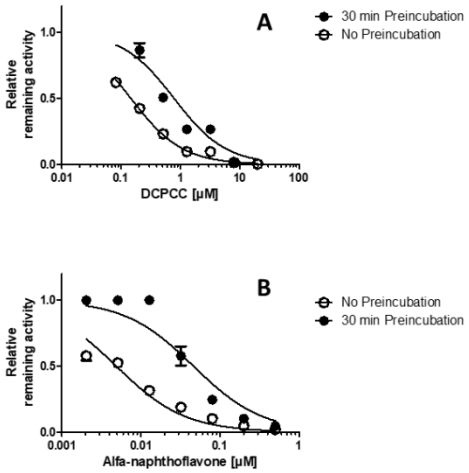

Figure 3.

cbdd_13669_f3.tif

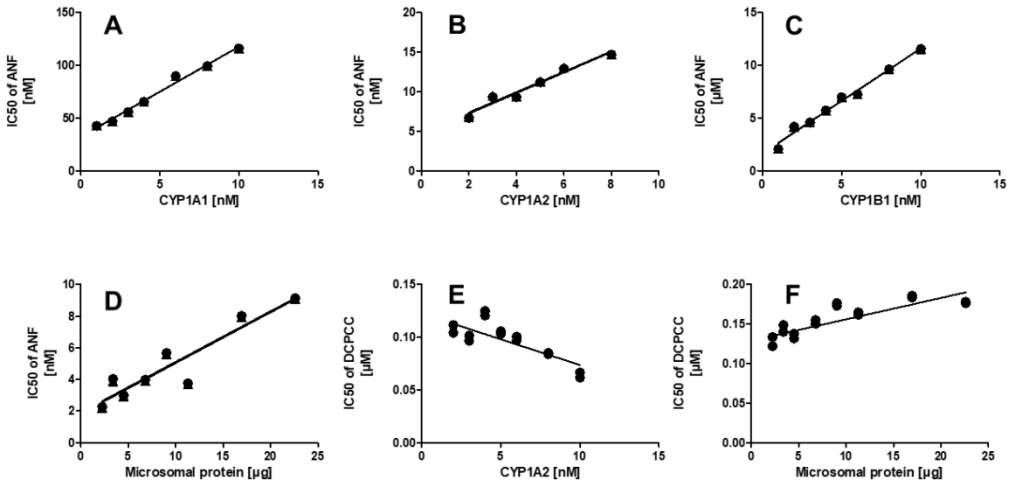

Figure 4.

cbdd_13669_f4.tif

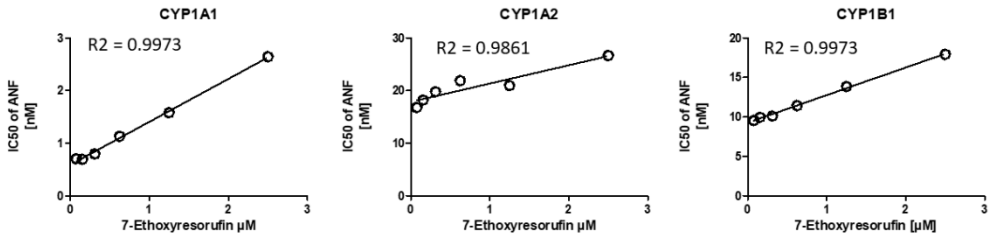

Figure 5.

cbdd_13669_f5.tif

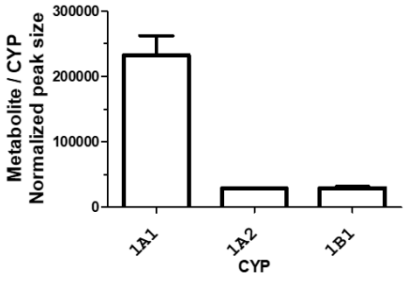

Figure 6.

cbdd_13669_f6.tif

Figure 7.

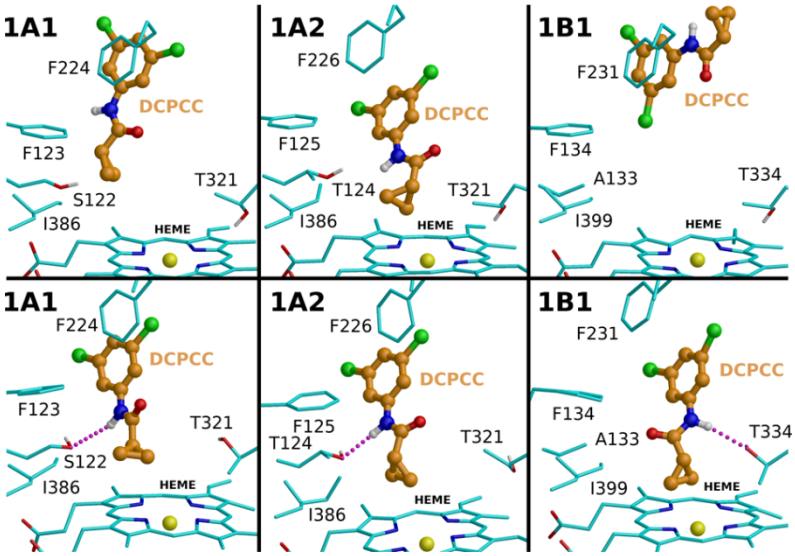

cbdd_13669_f7.tif

Figure 8

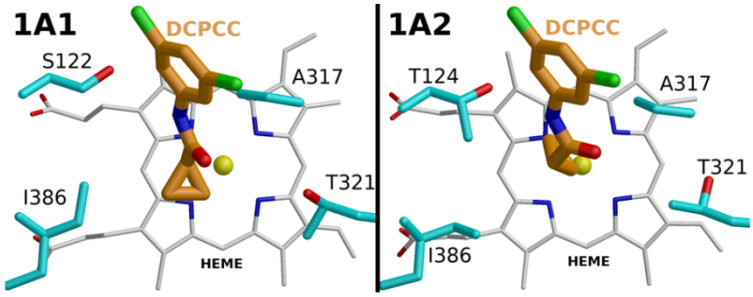

cbdd_13669_f8.tif

Figure 9

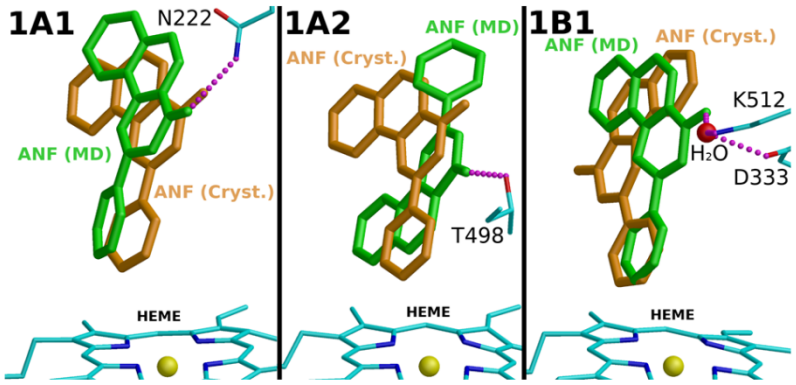

cbdd_13669_f9.tif